Int. J. Heat Mass Transfer. Vol. 36, No. 17, pp. 4151–4162, 1993
Printed in Great Britain

0017-9310/93 $6.00 + 0.00

Measurement of mass and momentum transport in wavy-laminar falling liquid films

ISSAM MUDAWAR† and RONALD A. HOUPT
Boiling and Two-Phase Flow Laboratory, School of Mechanical Engineering, Purdue University, West Lafayette, IN 47907, U.S.A.

(*Received* 24 *August* 1992 *and in final form* 18 *May* 1993)

Abstract—Experiments were performed to assess the role of large waves in the transport of mass and momentum in falling liquid films. Simultaneous two component velocity and film thickness measurements were made in wavy laminar films falling on the exterior of a vertical column. Solutions of water and propylene glycol, used as the working fluid in order to create relatively thick viscous films, yielded wavy laminar films over a Reynolds number range of 209 to 414. Examination of these conditions revealed that large waves behave as lumps of liquid sliding over a continuous substrate. Velocity fields within the substrate displayed reduced sensitivity to the large waves with increases in substrate thickness or reductions in dynamic viscosity. Furthermore, time traces of steam-wise velocity in the substrate were found to loosely resemble traces of film thickness, with fluctuations in velocity lagging fluctuations in thickness. By decomposing the stream-wise and radial velocity components into mean, wave induced velocity fluctuations, and turbulent fluctuations, a determination could be made as to whether these films were truly wavy laminar or turbulent. It is shown that, in wavy laminar films, a large portion of the flow, 40–70%, is transported by large waves.

1. INTRODUCTION

GIVEN the importance of falling liquid films in devices such as condensers, evaporators, and chemical reactors, a clear and quantitative understanding of the fluid mechanics of such films is desirable. Corresponding to this need, decades of work have been devoted to their study, but very little work has been done towards actually measuring velocities within *wavy* falling liquid films and correlating such information with the shape of the free interface. A brief history of work relating to this difficult task begins with Wilkes and Nedderman [1] who used a technique known as stereoscopic photography to measure the velocities of small bubbles suspended in aqueous glycerol or liquid paraffin diluted with petroleum ether. They studied both smooth and wavy laminar films of Reynolds numbers below five and noted that the profiles measured within wavy films were approximately parabolic. Unfortunately, their experimental apparatus and technique did not allow them to determine at which stream-wise location within a wave their measurements were taken.

Ho and Hummel [2] used a ruby laser to trigger the formation of a dye trace which they photographed at successive intervals in time. For their test fluids they used aqueous alcohol and alcohol–glycerol mixtures over a Reynolds number range from 124 to 2800. Their measurements revealed that the velocity profiles were parabolic with different coefficients for different Reynolds numbers. However, as with Wilkes and Nedderman, they could not determine the stream-wise location within a wave where their data were acquired.

Nakoryakov *et al.* [3] traced aluminum particles in water–glycerin films formed on the outside of an upright column with stroboscopic, stereoscopic photography. They tested their apparatus with smooth films of Reynolds numbers between 32 and 120. They also examined wavy films with *Re* between 20 and 58. The waves in these films were created by pulsations in the discharge upstream of the column. Unlike previous studies, they could determine the stream-wise location along a wave where their measurements were made and found the maximum deviation from a parabolic profile to be 15% in waves having a very steep front and gently sloping back. Although an improvement over previous studies, they could not accumulate and correlate large amounts of data in order to provide accurate statistical information.

Semena and Mel'nichuk [4] obtained single component laser-Doppler velocimetry measurements in planar falling liquid films. Their mean velocity data were obtained with distilled water and, like the data of Ho and Hummel, formed a parabolic profile whose precise shape was dependent upon the Reynolds number. Semena and Mel'nichuk made no attempt to correlate instantaneous velocity with the shape of the free interface. Additionally, they did not provide a description of their apparatus or measurement technique.

Since measuring the velocity fields in wavy falling liquid films has proven to be extremely difficult and little experimental information exists, some numerical

† Author to whom all correspondence should be addressed.

NOMENCLATURE

$C(\tau)$	cross-covariance function
g	acceleration due to gravity
f	frequency
$\dot{m}$	mass flow rate
N	total number of points within a time series
r_0	outer radius of column
Re	Reynolds number, $4\Gamma/\mu$
$R(\tau)$	autocovariance function
s	random variable which is a function of time
$\bar{s}$	mean value of s
$S(f)$	autospectrum
t	time
u	stream-wise velocity
U_W	velocity of large waves
u_w	fluctuating component of stream-wise velocity induced by waves
$\bar{u}$	mean stream-wise velocity
u'	fluctuating component of stream-wise velocity due to turbulence
u_*	friction velocity, $\sqrt{(\nu[\partial u/\partial y]_{y=0})}$
v	radial or cross-stream velocity
v_w	fluctuating component of radial velocity induced by waves
$\bar{v}$	mean radial velocity
v'	fluctuating component of radial velocity due to turbulence
$W(f)$	cross-spectrum
x	stream-wise distance measured downstream from the bottom of the porous section
y	distance normal to the wall measured outward from the wall
y_p	y location of the LDV probe volume.

Greek symbols

Γ	mass flow rate per unit width, $\dot{m}/(2\pi r_0)$
δ	film thickness
δ_s	maximum substrate thickness
$\bar{\delta}$	mean film thickness
μ	dynamic viscosity
ν	kinematic viscosity
ρ	fluid density
ρ_g	air density
σ^2	variance when used in statistical functions
τ	time delay when used in statistical functions
τ_w	wall shear.

work has been done. Bach and Villadsen [5] applied a finite element method to a wavy laminar film and solved the Navier–Stokes equations from a Lagrangian point of view. They found the stationary wave profile which develops from an initially small perturbation imposed on a smooth film flowing down a vertical wall. Their study spanned a Reynolds number range from 10 to 100 and compared well with actual data regarding wave celerity.

Brauner *et al.* [6] analytically explored the variation of interfacial velocity along a wave. In their paper, they discuss the existence of both extremum values and interfacial stagnation points. Extremum values correspond to a condition where the interfacial velocity does not exceed the wave velocity at any point along the wave. On the other hand, if the wave velocity is exceeded by the interfacial velocity, stagnation points occur and a circulating eddy resides within the wave. Each case is illustrated in Fig. 1(a) where the wave is considered stationary and the wall is moving upward at a velocity equal to the wave velocity. Maron and Brauner [7] presented both a finite difference and finite element analysis of an assumed wave form. Their analysis indicated that the velocity profiles at various locations along a wave were similar for small amplitude waves or ripples while stagnation points occurred for larger amplitude waves. In short, the appearance of a recirculation zone depended mainly upon the amplitude to substrate thickness ratio.

Recently, Lyu and Mudawar [8] measured, simultaneously, local thickness and liquid temperature of falling water films using a thermal conductance thickness probe and fast response thermocouples. They detected some periodicity in the film waviness with each large wave followed by a thin film. As shown in Fig. 1(b), the temperature profile was steep in the thin film and the near-wall region beneath the large wave and fairly flat within the wave itself. This suggests liquid in the large waves behaves as an isolated lump undergoing recirculation instead of continually mixing with the thin film. This observation poses a question of paramount importance to most thermal systems utilizing falling liquid films: how much of the film mass is transported by the large waves?

The present study attempts to assess the role of waviness in the transport of mass and momentum in falling liquid films through laser-Doppler velocimetry measurements. These velocity measurements are correlated to the shape of the free interface as determined by a parallel wire film thickness probe. The remainder of this paper will discuss the experimental techniques used and the results obtained.

2. EXPERIMENTAL FACILITIES

The falling film was formed on the exterior of a vertical column through the use of a 50 mm o.d., 610 mm long porous tube. The actual test section consisted of a 50 mm o.d., 2136 mm long poly-

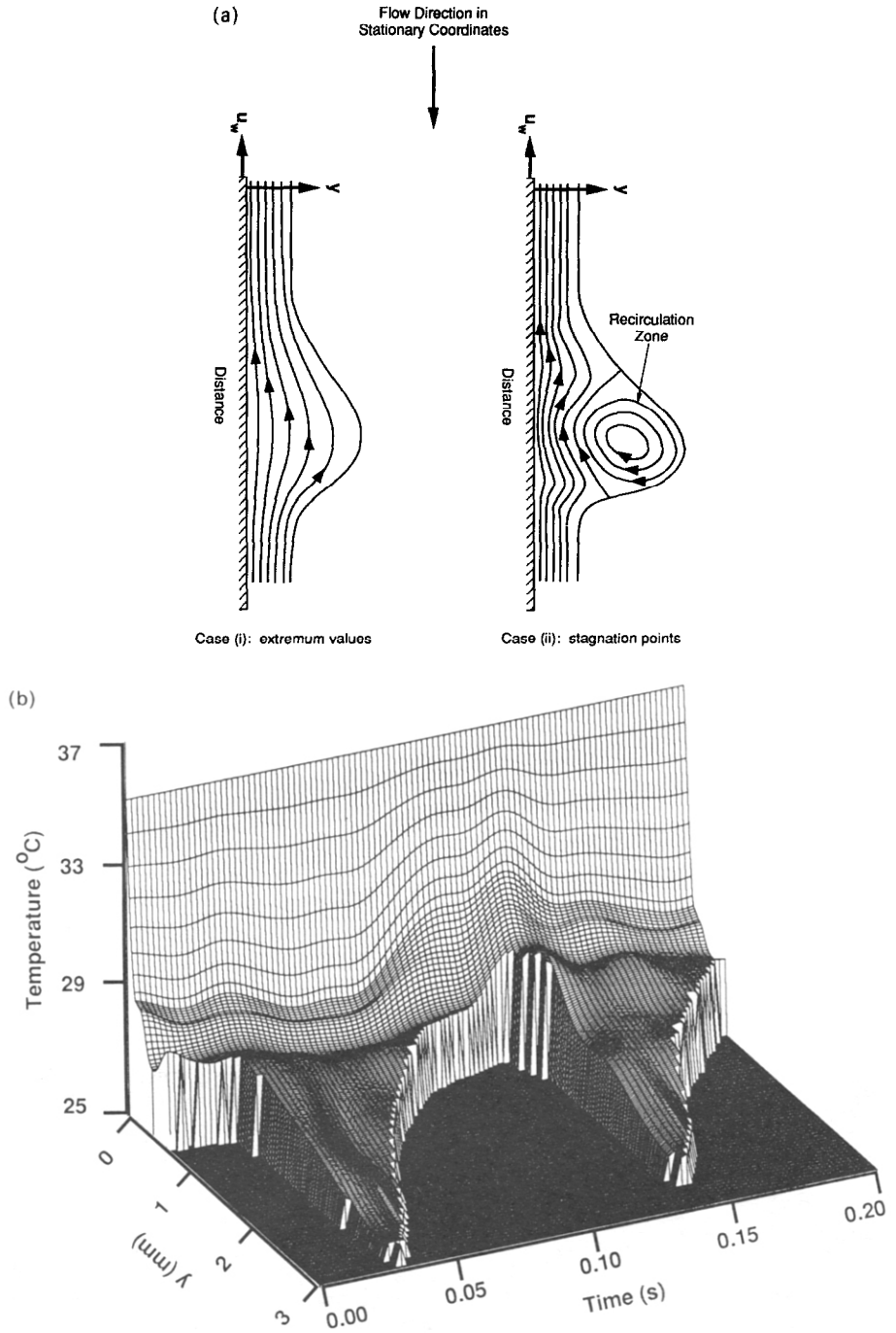

FIG. 1. (a) Streamlines plotted in wave coordinates (adapted from Brauner *et al.* [6]). (b) Liquid temperature variation with distance from the wall in a heated water film at $Re = 5700$ (adapted from Lyu and Mudawar [8]).

propylene tube installed immediately beneath the porous tube. Before operating the flow loop, the column was aligned to a true vertical position by referencing three plumbs and cleaned with acetone. Both a film thickness probe and a film sampling channel were located on the test section or free fall column in order to allow simultaneous film thickness and velocity measurements at $x = 1842.5$ mm. The film thickness probe and its use remained largely unchanged from previous studies of film thickness described in detail by Koskie *et al.* [9]. The thickness probe consisted of two 0.08 mm diameter platinum/10% rhodium wires mounted with a 0.51 mm center to center spacing.

Since the laser light required for LDV work cannot be easily focused to a probe volume through the irregular surface of the falling film, a sampling channel was constructed to slice the film. A slice of film was

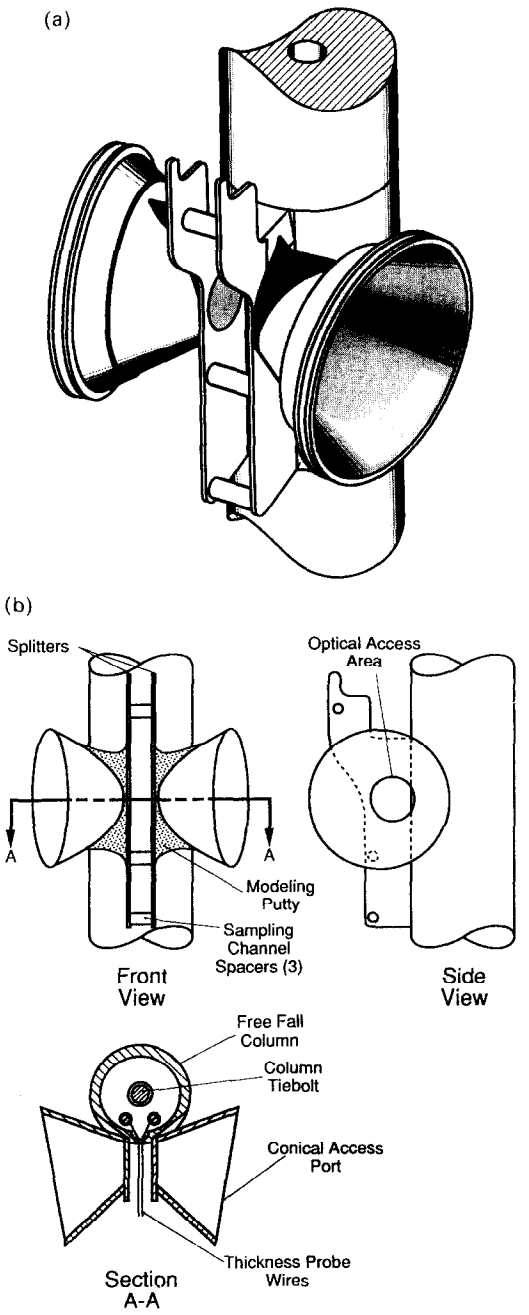

FIG. 2. Film sampling channel: (a) isometric view, (b) schematic drawing.

allowed to continue falling down the column while the rest of the film was moved out of the way of the laser beams. An isometric drawing of the sampling channel is shown in Fig. 2(a) while detailed views of the sampling channel are given in Fig. 2(b). The splitters were sharpened on the outside of the leading edges and spaced 12 mm apart so that the boundary layers formed on the splitters would not merge nor interfere with the LDV probe volume, and the splitters themselves would not interfere with the electrical field of the thickness probe. Geometric constraints of existing hardware decreed that the thickness probe wires

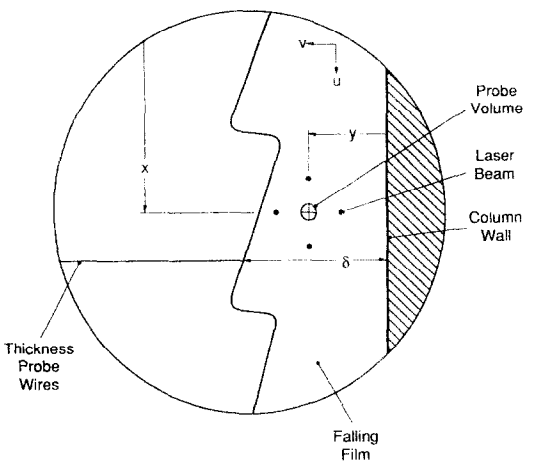

FIG. 3. Velocity and thickness measurements as seen through the conical access ports.

be located 28 mm downstream from the leading edges. The conical access ports shielded the laser beams from the liquid outside of the channel and allowed them to pass through each splitter and be focused within the film. Figure 3 shows the film as seen through the ports.

The actual LDV equipment consisted of a TSI System 9100-7 with a 2 W Argon-ion Lexel model 95 laser, a 4 beam system minus the beam stop and field stop hardware. The transmitting optics included a model 9117 lens with a focal distance of approximately 121.5 mm and a model 9188-A 2.27X beam expander. These components created a very small beam crossing, 0.029×0.150 mm. The system was assembled for forward scatter collection with the receiving optics stationed on the optical axis and traverses made in the radial direction (perpendicular to the column wall). Additionally, frequency shifting was utilized for both stream-wise and radial velocity measurements. Seeding was accomplished through the use of small air bubbles, 0.01 mm diameter, entrained in the liquid. Based upon calculation techniques given by Adrian *et al.* [10], even air bubbles 10 times that diameter would follow flow fluctuations of 1000 Hz frequency with an amplitude error of less than 0.01% in the fluids utilized in the current study.

The data acquisition system had the flexibility to be assembled in various configurations depending on the nature of the data being sought. Figure 4 illustrates how the system was implemented for simultaneous film thickness and two-component velocity measurements. The heart of the system was a Compaq 386 microcomputer with a 130 megabyte fixed disk and a 40 megabyte backup drive. Photomultipliers #1 and #2 were connected to TSI model 1980 counters #1 and #2, respectively. The analog outputs of the counters and the thickness probe circuitry were sampled by a HP 44702B high speed voltmeter installed in a HP 3852A Data Acquisition/Control Unit. This unit was connected with the Compaq through a MBC-488 GPIB interface card. Sampling was software controlled over a period of 10 s at 2000 Hz per channel

with only a 10 μs lag between channels. As previously determined by Karapantsios *et al.* [11], this sampling rate was more than sufficient to capture significant frequencies in the film thickness signal. Additionally, such a high rate allowed very good resolution of the wave forms themselves. This configuration was used for all wavy films investigated. Mean error in the LDV velocity measurements was estimated to be $\pm 0.5\%$.

3. RESULTS

In order to create relatively thick films and study the effects of viscosity, wavy films of $Re = 209$ and 410 were investigated with a water/90% propylene glycol solution while a Reynolds number of 414 was examined with water/70% propylene glycol. For each condition, simultaneous film thickness and two-component velocity measurements were obtained as a function of time. Figure 5(a) illustrates how the stream-wise velocity, or u component, increases in magnitude with both increases in film thickness and distance from the wall to the LDV probe volume, y_p. Additionally, the velocity increase tends to lag the film thickness increase by a few milliseconds. These same trends are observed in Fig. 5(b) for the 90% glycol solution at $Re = 410$ and in Fig. 5(c) for the 70% glycol solution at $Re = 414$. If all three figures are compared, however, it is apparent that the relationship between film thickness and stream-wise velocity is weakened by a reduction in viscosity. Furthermore, it is important to note how intermittency in the velocity signal corresponds to the LDV probe volume entering and exiting waves in all three cases.

Two important features demonstrated by Fig. 5(a) concerning just film thickness should also be pointed out. First, the majority of waves have a very steep front and a gradually sloping tail, a sawtooth pattern. Second, there is a depth beneath which liquid is always present. This area is loosely termed the substrate. As can be seen, the waves are not always equally spaced nor are they always the same size. Figure 5(b) demonstrates the effects of increasing the Reynolds number through an increase in flow rate. As shown, the same sawtooth pattern is found but with small waves or ripples superimposed on the large wave structure. Further examination also reveals that the substrate thickness has been increased. Testing at the same Re with a fluid of lower viscosity, the 70% glycol mixture, yielded the thickness trace shown in Fig. 5(c). Two main differences are noted between Figs. 5(b) and (c). First, the sawtooth wave shape is still present in the lower viscosity fluid but it is not quite as dominant as it is for the 90% glycol solution. Second the substrate thickness is smaller for the 70% glycol mixture.

Although the radial velocity component was measured, its magnitude was very small in all cases, less than approximately 1 cm s^{-1}. This was verified through the use of video tapes taken with an EktaPro 1000 high-speed motion analyzer. By placing the video camera at the same location used for the LDV receiving optics and placing a high power flood lamp behind a translucent plastic board at the transmitting optics location, filming was accomplished at 1000 frames per second. These tapes did not reveal any significant radial velocities. More significantly, examination of the tapes indicated that the large waves behaved like lumps of liquid sliding over the substrate. It should be noted that these observations are consistent with those of Lyu and Mudawar [8] who found temperature profiles within large waves to be flat. That is, the fluid within a wave behaved as an isolated lump containing a region of recirculation.

Statistical results

In an effort to quantify the preceding observations, a statistical analysis was performed on the film thickness signal and all *continuous* stream-wise velocity signals. This analysis consisted of autocovariances,

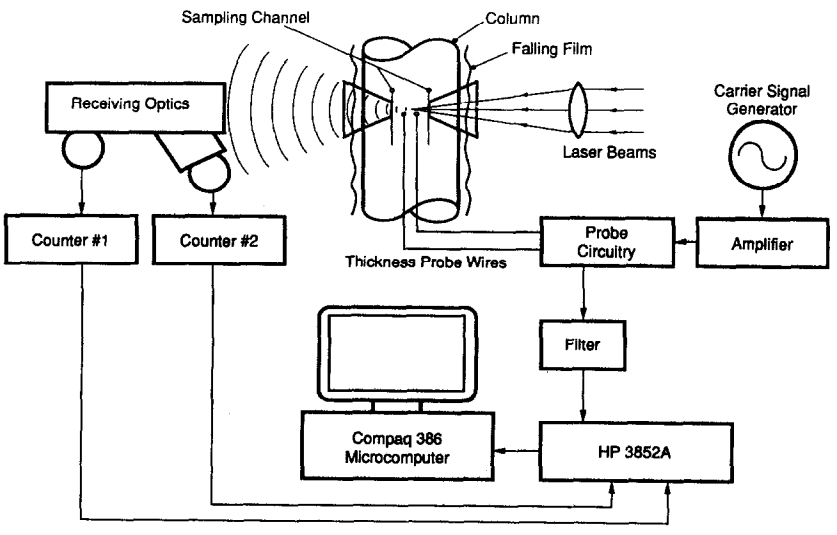

FIG. 4. Data acquisition system.

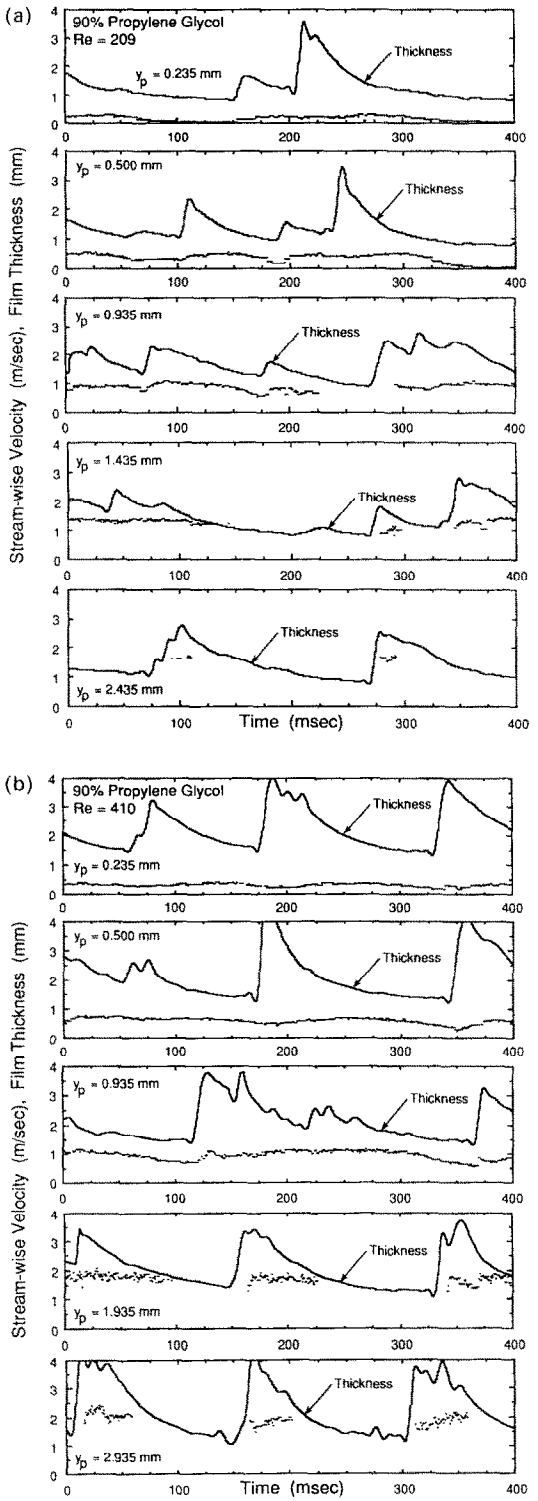

FIG. 5(a), (b).

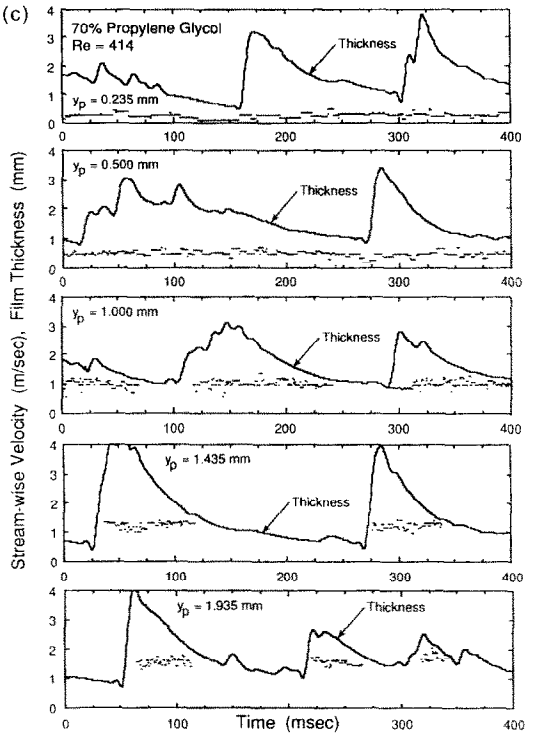

FIG. 5. Time records of film thickness and stream-wise velocity for: (a) 90% glycol at $Re = 209$, (b) 90% glycol at $Re = 410$, (c) 70% glycol at $Re = 414$.

$R(\tau)$; cross-covariances, $C(\tau)$; cross-variation plots; autospectra, $S(f)$; and cross-spectra, $W(f)$. Denoting a time series by s, $\bar{s}$ as the mean, σ^2 as the variance, N as the total number of points in the series, and τ as time delay, the relevant mathematical parameters can be defined as follows:

$$\bar{s} = \frac{1}{N}\sum_{i=1}^{N} s_i(t) \tag{1}$$

$$\sigma^2 = \frac{1}{N}\sum_{i=1}^{N} [s_i(t) - \bar{s}]^2 \tag{2}$$

$$R(\tau) = \frac{1}{N\sigma^2}\sum_{i=1}^{N} [s(t) - \bar{s}][s(t+\tau) - \bar{s}] \tag{3}$$

$$C(\tau) = \frac{1}{N\sigma_1\sigma_2}\sum_{i=1}^{N} [s_1(t) - \bar{s}_1][s_2(t+\tau) - \bar{s}_2] \tag{4}$$

$$S(f) = \int_{-\infty}^{\infty} R(\tau)\exp(-j2\pi f\tau)\,d\tau \tag{5}$$

$$W(f) = \int_{-\infty}^{\infty} C(\tau)\exp(-j2\pi f\tau)\,d\tau. \tag{6}$$

Since both film thickness and stream-wise velocity demonstrated repeating and related characteristics, computations of cross-covariance for y locations where the LDV probe volume was always submerged proved revealing. The cross-covariance is valuable in determining how much two time series resemble each other and the phase shift occurring between them. As displayed in Fig. 6(a), the velocity traces exhibited a strong resemblance to the film thickness records for the 90% glycol solution at a Reynolds number of 209 and time delay of approximately 0.04 s. Furthermore, the resemblance grew stronger as y_p was increased while the time delay remained unchanged. The evi-

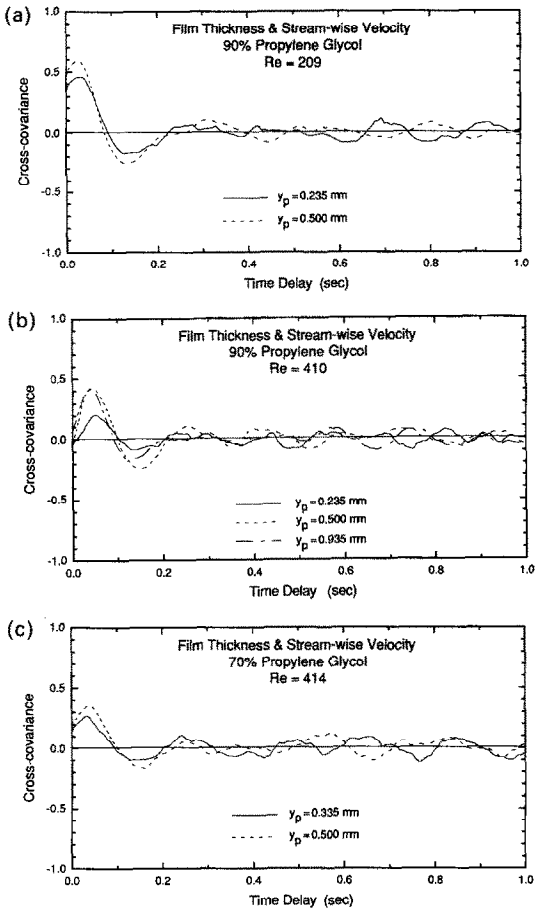

FIG. 6. Cross-covariance of film thickness and stream-wise velocity for: (a) 90% glycol at $Re = 209$, (b) 90% glycol at $Re = 410$, (c) 70% glycol at $Re = 414$.

dence that peaks in velocity, especially near the wall, occur a short time after peaks in film thickness agrees with the traces discussed earlier and with the work of Maron and Brauner [12]. These investigators simultaneously measured film thickness and the instantaneous mass transfer rate between the film and an inclined plate. They noted that the mass transfer rate peaked shortly after film thickness. Moreover, since the shear stress at the wall is given by

$$\tau_w = \mu \left[\frac{\partial u}{\partial y}\right]_{y=0} \tag{7}$$

and

$$\frac{\partial u}{\partial y} \approx \frac{u}{y} \tag{8}$$

for small y, the cross-covariance of stream-wise velocity measured at $y_p = 0.235$ mm is indicative of the cross-covariance of wall shear and further supports the work of Maron and Brauner.

Increasing the Reynolds number of the water/90% propylene glycol solution to 410 resulted in weakened resemblances, especially near the wall, and slightly larger time lags or phase shifts as depicted in Fig. 6(b). Figure 6(c) demonstrates how using the lower viscosity fluid weakened the resemblance even further but did not significantly affect the time lag. These results make sense when the waves are viewed as lumps of fluid sliding over a substrate. A lump moving periodically over the relatively thin substrate of a highly viscous fluid (water/90% propylene glycol, $Re = 209$) would influence the velocity fields within the substrate more than a lump moving over a thick substrate (90% glycol, $Re = 410$) or the substrate of a less viscous fluid (70% glycol, $Re = 414$).

Autocovariances, useful for determining how well a time series repeats itself, revealed fairly strong periodicity in both film thickness and stream-wise velocity. Consistent with the aforementioned cross-covariances, periodicity grew stronger as y_p was increased and grew weaker with increasing flow rate or decreasing viscosity.

Since the cross-covariance plots revealed that some correlation did exist between film thickness and stream-wise velocity, the two quantities were plotted against each other. These plots, henceforth called cross-variation plots, are shown in Figs. 7(a)–(c). As evident from these graphs, a strong relationship existed between velocity and film thickness until the thickness increased beyond a certain value. Furthermore, increasing the Reynolds number of the 90% glycol solution from 209 to 410 slightly weakened this correlation. The effects of lowering the viscosity are shown in Fig. 7(c). As previously observed, the lower viscosity 70% glycol mixture exhibited a much more feeble relationship between film thickness and stream-wise velocity for a nearly identical Reynolds number of 414. The physical significance of the linear region observed in each plot can be explained most easily by examining the fully developed velocity profile of a laminar, planar, falling liquid film. According to Nusselt [13], this profile is given by:

$$u = \frac{g(\rho - \rho_g)}{\mu}\left[y\delta - \frac{y^2}{2}\right] \tag{9}$$

which, for a constant value of y, expresses the stream-wise velocity as a linear function of δ, the film thickness. In light of equation (9), the linear region of Figs. 7(a)–(c) can be attributed to changes in the substrate thickness between large waves. Moreover, equation (9) indicates that the slope should increase as y is increased, and this trend is observed in Fig. 7(a) where the correlation between film thickness and velocity is the strongest. The horizontal region of data scatter in each plot may be ascribed to large waves sliding over the substrate, and it may be concluded that the substrate tends to thicken in the vicinity of large waves since the horizontal region connects only with the upper portion of the linear regime. These deductions are further supported by referring back to Figs. 5(a)–(c). As illustrated, the stream-wise velocity does not follow the trends in film thickness exactly, but it does increase as a wave or group of waves pass the meas-

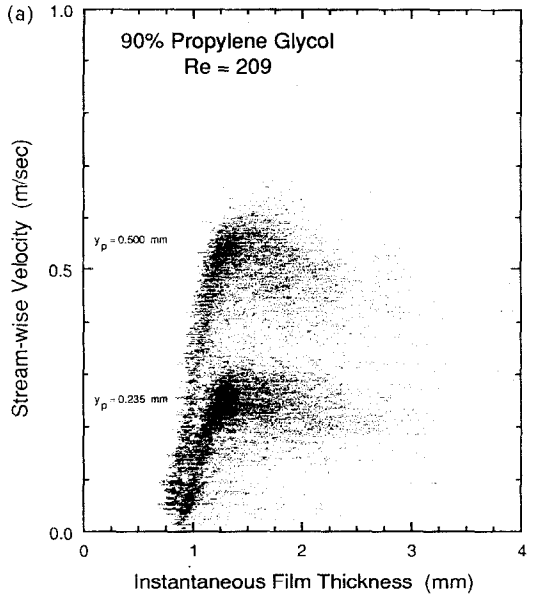

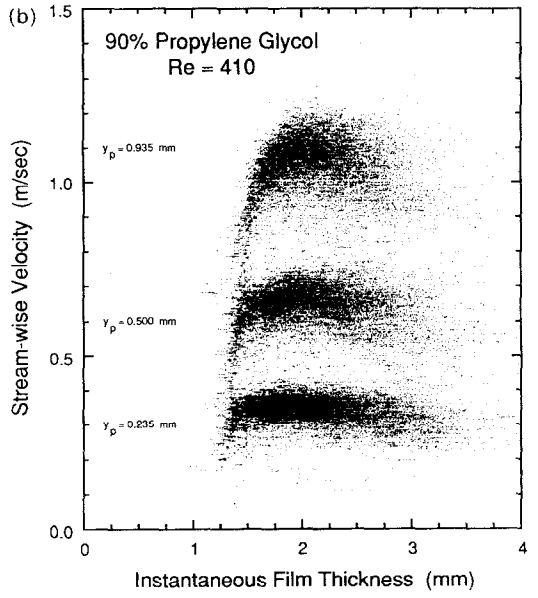

FIG. 7(a), (b).

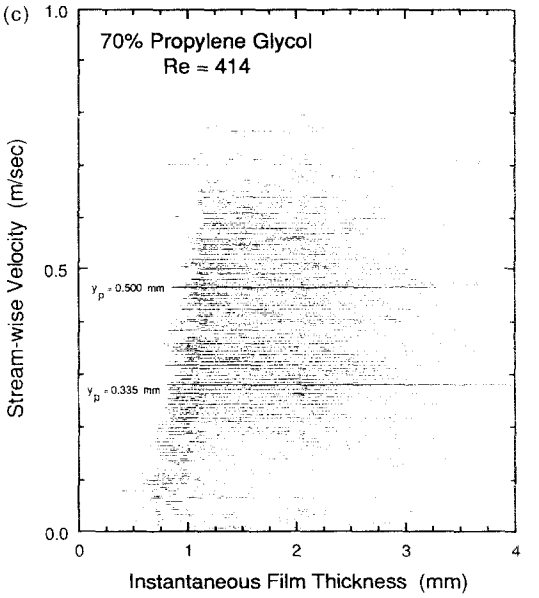

FIG. 7. Illustration of the relation between film thickness and stream-wise velocity for: (a) 90% glycol at $Re = 209$, (b) 90% glycol at $Re = 410$, (c) 70% glycol at $Re = 414$.

uring volume. Thus, the stream-wise velocity within the substrate is influenced by the waves through their effect on the substrate thickness. This also helps explain the strong, but not perfect, correlation between film thickness and velocity observed in the cross-covariance plots.

Figures 8(a)–(c) illustrate the result of examining film thickness and stream-wise velocity traces in the frequency domain. A Hanning window, as outlined by Bendat and Piersol [14], was applied to the data before being processed with a Fast Fourier Transform routine given by Newland [15]. Only frequency components whose magnitudes were greater than 1% of the maximum component are shown. As presented for water/90% propylene glycol at $Re = 410$, the range of

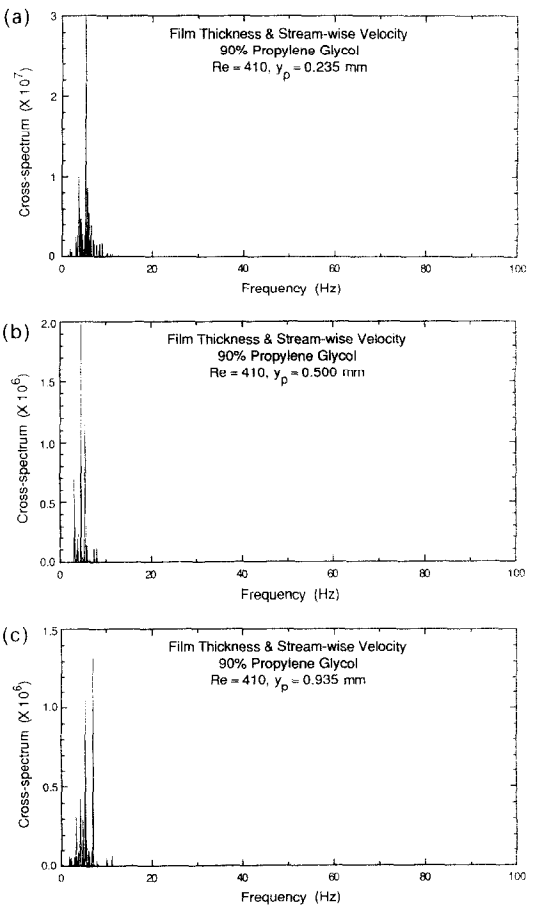

FIG. 8. Cross-spectra from 90% glycol at $Re = 410$ between film thickness and (a) u at $y_p = 0.235$ mm, (b) u at $y_p = 0.500$ mm, (c) u at $y_p = 0.935$ mm.

dominant frequencies in the cross-spectrum was 0 to 10 Hz for each y_p. Although not shown, the same range was found for water/90% propylene glycol at $Re = 209$ and water/70% propylene glycol at $Re = 414$. Autospectra computed for each condition revealed significant frequencies in the range of 0–10 Hz for 90% glycol at $Re = 209$, 0–20 Hz with peaks below 10 Hz for 90% glycol at $Re = 410$, and 0–30 Hz with peaks below 10 Hz for 70% glycol at $Re = 414$. The band of dominant frequencies for film thickness was 0–20 Hz in each of the three cases. Since the range of significant frequencies in film thickness was always found to be higher than the range corresponding to velocity or cross-spectra, these observations are compatible with the previous discussion concerning the effect of waves on cross-variation plots. That is, waves influence substrate velocity indirectly through their influence on substrate thickness. Momentum is transferred from the wave of 'sliding lump' in a diffusive manner into the substrate.

Turbulence results

Since a definite relationship between film thickness and stream-wise velocity was found to exist, the total stream-wise velocity was decomposed into three components: mean velocity, wave induced velocity fluctuations, and turbulent fluctuations. These components are referred to as $\bar{u}$, u_w, and u', respectively. A very similar concept has been used by Howe *et al.* [16]. In the present investigation, separation of the components was accomplished through the use of a low pass digital filter with a very sharp cutoff frequency as discussed by Walraven [17]. The actual cutoff frequency was determined by manual inspection of the velocity traces, referencing the auto and cross-spectra, and performing several iterations for each velocity record. Through this process, it was found that the cutoff frequency did not change appreciably with changes in y location but did change with Reynolds number. Figure 9 shows an example of the separation process. As shown, the velocity signal could be decomposed into a mean component, a wave induced component which reflected large instantaneous velocity excursions, and a 'turbulent' component which reflected high frequency/low amplitude excursions. Examination of u_w proved very helpful when analyzing data from the water/70% propylene glycol solution. For example, since the 70% glycol data yielded poor cross-covariances with regard to total stream-wise velocity, these statistical quantities were recomputed for just the u_w component. As shown by Fig. 10, each u_w trace exhibited a more substantial resemblance with the corresponding film thickness trace while the time lags remained approximately the same.

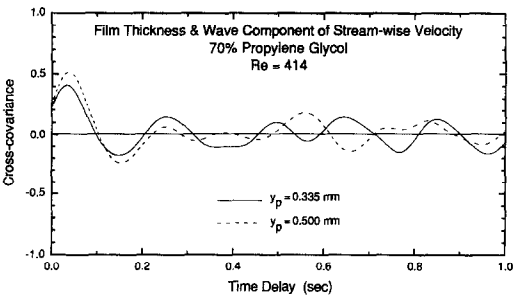

FIG. 10. Cross-covariance for 70% glycol at $Re = 414$ utilizing film thickness and u_w.

Another application of velocity decomposition is depicted in Fig. 11 where turbulence induced shear is compared with the wall shear due to dynamic viscosity. In executing these computations, the same cutoff frequency used on u was also applied to the

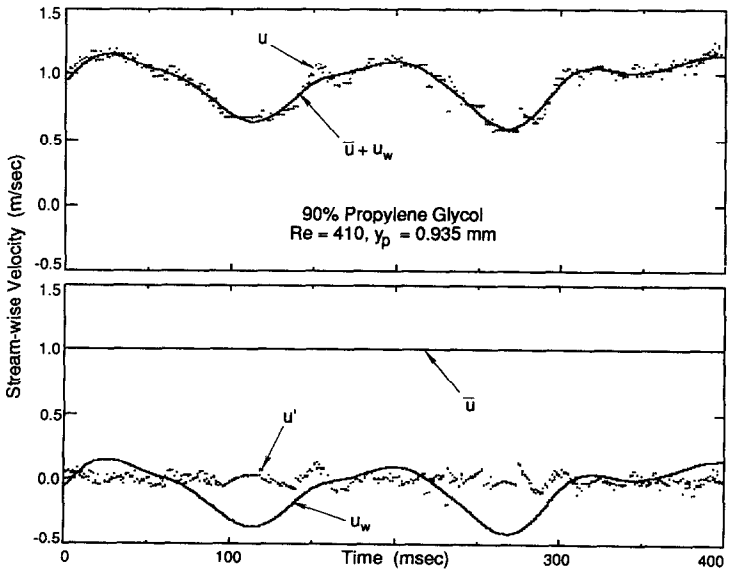

FIG. 9. Separation of u into the components: $\bar{u}$, u_w, and u'.

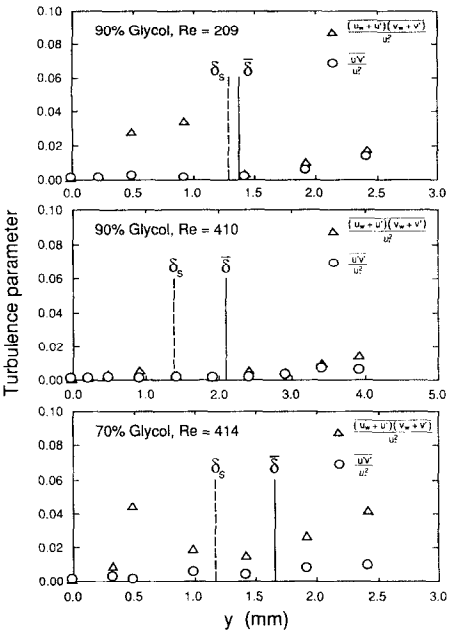

FIG. 11. Turbulence in wavy films.

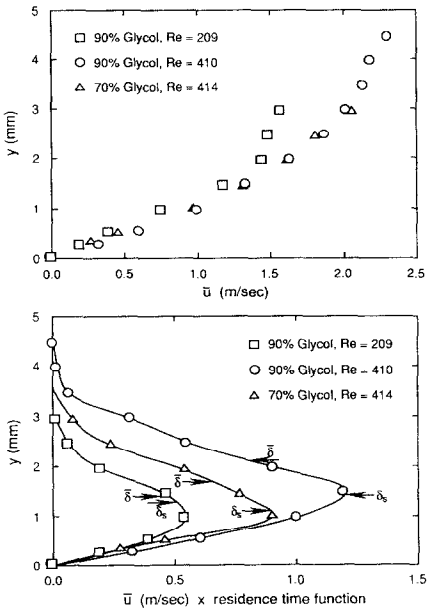

FIG. 12. Mean velocity profiles in wavy films.

radial velocity, while the wall shear was determined from a polynomial curve fit of the mean velocities measured at points which were always submerged. In all three cases, the computations of turbulence induced shear were performed with and without the wave induced fluctuating components. The results turned out to be very small either way. In addition, the plots display how $\overline{u'v'}/(u^*)^2$ was always smaller than $(\overline{u_w+u'})(\overline{v_w+v'})/(u^*)^2$, and that these films were wavy yet laminar.

Velocity profile across the film

Mean velocity profiles are illustrated in Fig. 12. In the upper plot, mean velocity was computed by time averaging the stream-wise velocity signal over only those periods when the LDV probe volume was submerged within the liquid film. Data obtained at a Reynolds number of approximately 400 were nearly the same for both the 90 and 70% glycol solutions while that obtained at $Re = 209$ for 90% glycol exhibited lower velocities. The lower figure was obtained by multiplying the previously determined mean velocities by a residence time function, the time during which the LDV probe volume was submerged divided by the total measurement time. As demonstrated, the mean velocity calculated in this manner began to decrease near the vicinity of the maximum substrate thickness, δ_s, determined from cross-variation plots, Figs. 7(a)–(c). This makes good sense when one considers that the probe volume resides outside the film for significant periods of time when placed at y locations beyond such a thickness. By performing numerical integrations, this figure also reveals that a large portion of the mass flow rate was transported within waves: 40% for 90% glycol at $Re = 209$, 67% for 90% glycol at $Re = 410$, and 48% for 70% glycol at $Re = 414$.

In order to gain insight into velocity profiles at different stream-wise locations within a wave, waves of the same size and shape were overlaid as illustrated in Fig. 13. Isolated, sawtooth shaped waves were picked since they were found to be very common as shown previously. This entire procedure was necessary since LDV measurements could be obtained at only one y location at a time. As can be seen for water/90% propylene glycol at $Re = 410$, the velocity profile for $t = 2.5$ ms was nearly parabolic. Later, at $t = 20$ ms, a body of high velocity fluid passed the measurement location yet the profile near the wall retained its parabolic shape. Between the high velocity fluid and near-wall fluid is an interface of vanishing shear stress, evidence of the large wave simply sliding over the substrate. At $t = 52.5$ ms, the 'lump' of fluid was beginning to exit the probe volume and the profile near the wall showed signs of acceleration. That is, the stream-wise velocity increase lagged the increase in film thickness. Finally, the fluid near the wall decelerated by $t = 119$ ms, well after the wave peak had passed. Although not shown, a similar behavior was observed for 90% glycol at $Re = 209$ and 70% glycol at $Re = 414$. Consistent with the observations and results of previous sections, the effects of a fluid lump were not felt as strongly within the thicker substrate created by larger flow rates or within the thinner substrate of a lower viscosity fluid, however, they were still present.

Disappearance of wavy laminar regime

The authors have also performed studies on mass and momentum transport in falling films of the same fluids employed in the present study but at much higher Reynolds numbers. Increasing Re above about 2650 for 70% glycol and 1400 for 90% glycol was found to completely dampen the film waviness, result-

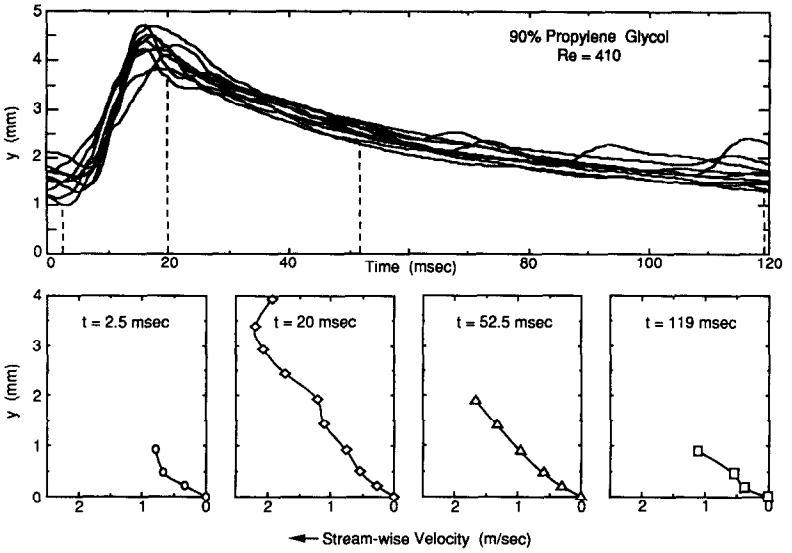

FIG. 13. Composite wave for 90% glycol at $Re = 410$.

ing in perfectly smooth and laminar films. This effect was attributed to thickening of the film at these high Reynolds numbers and to the increased length of the 'ripple free' entrance region for a finite column length. A detailed discussion of these issues can be found elsewhere [18].

4. SUMMARY

1. Simultaneous film thickness and two component velocity measurements performed in a water/90% propylene glycol film at Reynolds numbers of 209 and 410 and in a water/70% propylene glycol film at $Re = 414$, revealed that large waves moved as lumps sliding over a continuous substrate which grew in thickness as waves or groups of waves passed. This was further verified with a high-speed video motion analyzer.

2. Radial velocities were found to be very small for all three conditions, less than 0.01 m s^{-1}. This too was verified with a high-speed video motion analyzer.

3. Stream-wise velocities in the substrate were found to become less sensitive to waves as the substrate thickness was increased or as the fluid viscosity was lowered. In all cases, cross-covariances demonstrated a loose resemblance between film thickness time traces and stream-wise velocity time traces. The resemblance grew stronger with increasing distance from the wall. Furthermore, changes in stream-wise velocity lagged changes in films thickness.

4. When mean stream-wise velocities were multiplied by a residence time function, the resulting velocities were found to increase from the wall to the approximate maximum substrate thickness and decrease thereafter despite high stream-wise velocities recorded in the waves.

5. Large waves were determined to play a significant role in transporting liquid mass in wavy, falling liquid films, carrying 40–70% of the total mass flow rate for the conditions tested.

REFERENCES

1. J. O. Wilkes and R. M. Nedderman, The measurement of velocities in thin films of liquid, *Chem. Engng Sci.* **17,** 177–186 (1962).
2. F. C. K. Ho and R. L. Hummel, Average velocity distributions within falling liquid films, *Chem. Engng Sci.* **25,** 1225–1237 (1970).
3. V. E. Nakoryakov, B. G. Pokusaev, S. V. Alekseenko and V. V. Orlov, Instantaneous velocity profile in a wavy fluid film (English translation), *J. Engng Phys.* **33,** 1012–1016 (1977).
4. M. G. Semena and G. A. Mel'nichuk, Mean-velocity distributions in a falling film, *Fluid Mech.—Sov. Res.* **7,** 145–151 (1978).
5. P. Bach and J. Villadsen, Simulation of the vertical flow of a thin, wavy film using a finite-element method, *Int. J. Heat Mass Transfer* **27,** 815–827 (1984).
6. N. Brauner, D. M. Maron and I. Toovey, Characterization of the interfacial velocity in wavy thin film flow, *Int. Comm. Heat Mass Transfer* **14,** 293–302 (1987).
7. D. M. Maron and N. Brauner, Flow patterns in wavy thin films: numerical simulation, *Int. Commun. Heat Mass Transfer* **16,** 655–666 (1989).
8. T. H. Lyu and I. Mudawar, Statistical investigation of the relationship between interfacial waviness and heat transfer to a falling liquid film, *Int. J. Heat Mass Transfer* **34,** 1451–1464 (1991).
9. J. E. Koskie, I. Mudawar and W. G. Tiederman, Parallel-wire probes for measurement of thick liquid films, *Int. J. Multiphase Flow* **15,** 521–530 (1989).
10. R. J. Adrian, L. M. Fingerson and S. L. Kaufman, Laser velocimetry theory, application, and techniques, *TSI Short Course on Laser Doppler Velocimetry*, St. Paul, MN (1987).
11. T. D. Karapantsios, S. V. Paras and A. J. Karabelas, Statistical characteristics of free falling films at high Reynolds numbers, *Int. J. Multiphase Flow* **15,** 1–21 (1989).
12. D. M. Maron and N. Brauner, Characteristics of inclined thin films, waviness and the associated mass transfer, *Int. J. Heat Mass Transfer* **25,** 99–110 (1982).

13. W. Nusselt, Die oberflachenkondensation des wasserdampfes, *Z. Ver. Duet. Ing.* **60,** 541–546, 569–575 (1916).
14. J. S. Bendat and A. G. Piersol, *Engineering Applications of Correlation and Spectral Analysis*. Wiley, New York (1980).
15. D. E. Newland, *An Introduction to Random Vibration and Spectral Analysis* (2nd Edn). Longman, New York (1984).
16. B. M. Howe, A. J. Chambers, S. P. Klotz, T. K. Cheung and R. L. Street, Comparison of profiles and fluxes of heat and momentum above and below an air–water interface, *J. Heat Transfer* **104,** 34–39 (1982).
17. R. Walraven, Digital filters, *Proc. of the Digital Equipment Computer Users Society*. San Diego, CA (1980).
18. I. Mudawar and R. A. Houpt, Mass and momentum transport in smooth falling liquid films laminarized at relatively high Reynolds numbers, *Int. J. Heat Mass Transfer* **36,** 3437–3448 (1993).